RESEARCH ARTICLE

QUANTUM PHYSICS

Vortex beams of atoms and molecules

Alon Luski[1]†, Yair Segev[1]†‡, Rea David[1], Ora Bitton[1], Hila Nadler[1], A. Ronny Barnea[2], Alexey Gorlach[3], Ori Cheshnovsky[2], Ido Kaminer[3], Edvardas Narevicius[1]*

Angular momentum plays a central role in quantum mechanics, recurring in every length scale from the microscopic interactions of light and matter to the macroscopic behavior of superfluids. Vortex beams, carrying intrinsic orbital angular momentum (OAM), are now regularly generated with elementary particles such as photons and electrons. Thus far, the creation of a vortex beam of a nonelementary particle has never been demonstrated experimentally. We present vortex beams of atoms and molecules, formed by diffracting supersonic beams of helium atoms and dimers off transmission gratings. This method is general and could be applied to most atomic and molecular gases. Our results may open new frontiers in atomic physics, using the additional degree of freedom of OAM to probe collisions and alter fundamental interactions.

Vortices represent one of the clearest manifestations of angular momentum in nature, governing the hydrodynamics of the smallest insects, patterns of weather, and the motions of the stars in the galaxy. On all scales, vortices are characterized by the circulation of flux around an axis, whether the flux is composed of fluid mass in a classical eddy (*1*), magnetic field in a superconductor, or phase in a superfluid wave function (*2*). In quantum mechanics, a particle's angular momentum must have an integer value (*3*). Accordingly, the quantum manifestations of angular momentum are inherently different from the classical manifestations, contributing to selection rules in optical transitions, magnetic resonance spectroscopy, and the origins of the atomic fine structure. A particularly notable example of angular momentum is the quantized vortices often observed in a Bose-Einstein condensate (BEC) (*4*–*6*). In these, as well as in other vortices, the phase of the wave function varies around a singular point or axis, giving rise to a quantity called orbital angular momentum (OAM).

The quantization axis of the OAM in a vortex can also coincide with the propagation axis of a beam. Unlike vortices in a cold, confined BEC, which constitute an excitation of many atoms, a vortex beam consists of freely moving particles, each carrying intrinsic OAM that arises from the nontrivial shape of the single-particle wave function. Such vortex beams were first realized in experiments with photons (*7*), which have since found applications ranging from optical tweezers (*8*) to astrophysics (*9*), communication (*10*), and more (*11*, *12*). Electron vortex beams (*13*), first predicted and demonstrated two decades later (*14*), have been used, for example, to study chirality (*15*), magnetization mapping (*16*), and transfer of angular momentum to nanoparticles (*17*), and ongoing efforts include altering selection rules and controlling nuclear decay (*18*–*20*). Going beyond elementary particles such as the photon and electron, various proposals have been put forth for creating vortex beams of composite particles, such as neutrons (*21*), protons (*22*), and atoms (*23*, *24*), which are envisioned to alter the fundamental interactions of such particles and to enable probing of their internal structure. There have been experimental efforts to create neutron beams with OAM (*25*), which have been hindered by insufficient coherence lengths (*26*). Thus far, no experiment has created vortex beams of nonelementary particles.

Here, we present the first reported experimental demonstration of vortex beams with nonelementary particles, namely atoms and molecules of helium. Starting with a supersonic gas source, we created a beam of atoms with large transverse coherence lengths and diffracted them off a nanometric grating. The diffracted image revealed a series of ring-shaped patterns corresponding to nonzero OAM states of helium atoms. We further observed vortex beams of metastable helium dimers, a molecule formed in the supersonic expansion of the atomic gas after an electrical discharge. Although we used metastable helium beams for efficient and spatially resolved detection, our method could be generally applied to any supersonic beam of atoms or molecules and might be applicable to create vortices of ions and protons.

The common path to imparting OAM on particles in a beam is through waveform shaping—modifying an incoming plane wave's amplitude and phase to produce the desired wave. Before shaping, the wave function of a free particle propagating along the z axis can be described by $\psi'(r,z) = f'(r)e^{ikz}$, where $f'(r)$ is the transverse radial distribution and k is the particle's wave number. The characteristic dimension of the transverse distribution is defined by the coherence length Δ_c, a length scale dictated by the uncertainty in the transverse position of a particle. The phase of $\psi'(r,z)$ is uniform in each plane normal to the z axis and is modulated along z according to the wave number, $k = 2\pi/\lambda$. For a particle with mass m, $\lambda = h/mv$ is the de Broglie wavelength, where v is the propagation velocity and h is Planck's constant. Whereas the de Broglie wavelength can be only increased by reducing a particle's velocity, the coherence length can be manipulated by

[1]Faculty of Chemistry, Weizmann Institute of Science, Rehovot, Israel. [2]School of Chemistry, Sackler Faculty of Exact Sciences, Tel Aviv University, Tel Aviv, Israel. [3]Department of Electrical and Computer Engineering, Technion – Israel Institute of Technology, Haifa, Israel.
*Corresponding author. Email: edn@weizmann.ac.il
†These authors contributed equally to this work. ‡Present address: Department of Physics, University of California, Berkeley, Berkeley, CA, USA.

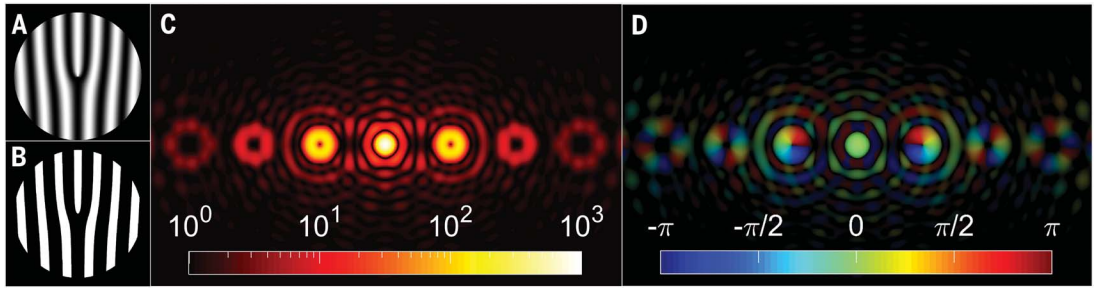

Fig. 1. Calculated diffraction image of vortex beams from a binary transmission grating. (**A** to **D**) The grating required to produce a vortex beam with a topological charge of $|l| = 1$, calculated from the interference between the target and reference wave, is shown in (A). For fabrication purposes, the calculated amplitude is binarized into slits with transmitting (white) and blocking (black) areas, with a forked edge dislocation in the center (B). This produces a series of vortices with topological charges $l = \pm1, \pm2, \ldots$, and in the far field, the intensity of the wave appears as a series of rings on either side of a central $l = 0$ spot (C). The hole in each ring coincides with a singularity in the phase of the function (D), around which the phase varies by $|2\pi l|$. The images were calculated for a grating with an open-to-blocked slit periodicity ratio of 40/60 and assuming that the coherence length of the beam is equal to the diameter of the circular aperture. Intensity in (C) is in arbitrary units.

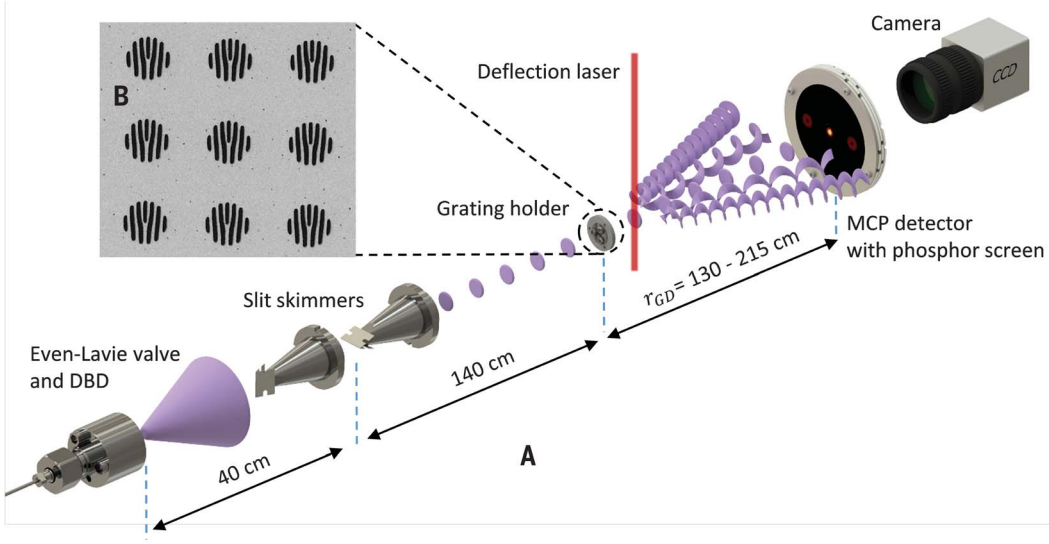

Fig. 2. Experimental setup for the production and detection of atomic and molecular vortex beams. (**A** and **B**) As shown in (A), a cooled Even-Lavie valve emits supersonic pulses of gas (purple cone), which are collimated by two slit skimmers to select the radial velocity spread and increase the transverse coherence length of the particles (purple disks). The beam impacts nanometric gratings, manufactured as an array of forked shapes (B), and is diffracted as vortex beams with different values of OAM (purple helixes). The metastable fraction of particles excited by the DBD in the valve decay upon interacting with the MCP, emitting light from a phosphor screen that is recorded on a camera. The impact point is localized in real time to high resolution, and the integrated image, assembled from hundreds of thousands of events, reveals the characteristic series of rings of OAM beams on either side of the central spot. When imaging the metastable dimers, a deflection laser beam resonant with an atomic transition of the triplet-state metastable atoms is crossed with the particles immediately after the grating (vertical red line), deflecting most of the detectable atoms to emphasize the dimer signal.

geometrical means. The desired outgoing vortex beam can be described by $\psi(r,z,\phi) = f(r)e^{ikz+il\phi}$, where ϕ is the azimuthal angle around the z axis and the integer l is termed the topological charge of the wave. Here, the constant phase wavefront is helical. Such a wave carries $l\hbar$ of OAM (*7*), where $\hbar = h/2\pi$. To achieve this shaping, several previous demonstrations of vortex beams of photons and electrons used spiral phase plates (*27*, *28*), which impart a single quanta $l\hbar$ of OAM on particles passing through them. However, fabricating such plates becomes challenging for beams of heavy particles with correspondingly shorter wavelengths, such as atoms and molecules, because of the required precision of the spiraling thickness profile. The spiral-plate method is further limited for atoms and molecules because of their low transmission probabilities through solid plates.

We followed an alternative approach, first demonstrated with vortices of light (*29*), and implemented transmission gratings designed by computer-generated holography. In this process, the required grating is designed by calculating the interference between the target wave—the vortex wavefunction—and a slightly tilted reference plane wave. The ideal theoretical grating contains a sinusoidal amplitude profile with an edge dislocation in the center, giving a "forked" shape (Fig. 1A). For fabrication, the amplitude profile was binarized, producing areas that either transmit or block the wave (Fig. 1B). The resulting binary gratings create a series of vortex beams with different topological charges with integer values $l = \pm n, \pm 2n, \ldots$. In a far-field plane parallel to the gratings, the intensity—or probability density, $|\psi|^2$—appears as a corresponding series of rings on either side of a central spot (Fig. 1C). The holes in these rings correspond to singularities in the phase of the wave function (Fig. 1D), with the phase changing by $|2\pi l|$ along a circle around a singularity with charge l. The number of edge dislocations, n, that fall within the transverse extent of an impacting particle's wave function (its coherence length) determines the spacing of the OAM values imparted into neighboring vortex beams, $n\hbar$.

Using such gratings, we have demonstrated the production of atomic vortex beams by gratings with one and two dislocations. We have also demonstrated molecular vortices produced by a single-edge dislocation grating with dimensions optimized for metastable helium dimers.

Experimental setup

We began by generating a supersonic beam of helium using a pulsed Even-Lavie valve (*30*). This source produces dense ensembles of particles with narrow velocity distributions. The longitudinal wavelength of the particles is controlled by changing the valve's temperature, where a lower temperature corresponds to a slower beam and thus a longer wavelength. We cooled the valve to 115 K to produce a beam with a mean velocity of v = 1090 m/s, corresponding to a de-Broglie wavelength of λ = 90 pm for helium atoms. We measured a longitudinal velocity spread of about 3% (full width at half-maximum), sufficiently low to avoid substantial chromatic aberrations in the diffraction image.

The pulse of atoms propagated until it diffracted off the transmission grating. Producing such diffraction gratings for beams of atoms or molecules requires fabrication of nanometric features, because the dimensions must correspond to the relatively small transverse coherence lengths associated with these particles (*31*–*35*). This coherence length is typically controlled by selecting the range of transverse velocities of the particles reaching the grating (*36*). In our experiment, we limited the radial spread by placing two perpendicular slit skimmers 40 cm downstream of the valve, allowing only a collimated beam to pass through their 150-μm apertures (Fig. 2A). The spread of the impacting particles was thus constrained by the solid angle covered by the skimmer apertures as viewed from the grating. For measurements aimed at imaging atoms, we set the distance between the skimmers and the grating to 140 cm to limit this divergence to a cone with a half-angle α = 55 μrad. For helium atoms, this corresponds to an average transverse coherence length of $\Delta_c = \lambda/2\alpha$ = 840 nm.

For our gratings, we constructed nanometric transmission holograms on 20-nm-thick silicon nitride membranes. The fabrication process is described in detail in the supplementary materials. Each hologram was etched in a circular area with a diameter a = 600 nm, and the grating slits were designed with a periodicity of d = 100 nm and approximately equal open and blocked areas, to give a diffraction angle of λ/d = 0.9 mrad for the l = ±1 orders. To increase the total intensity, the gratings repeated periodically every 1.2 μm over an area of 50 μm by 50 μm (Fig. 2B). The developed area was sufficiently small to avoid substantial incoherent blurring of the image in the far field, and the distance between holograms was chosen to be large enough to avoid coherent interference ("cross-talk") between paths through neighboring holograms. Details on the sources of blurring are given in the supplementary materials.

For detection, we used a dielectric-barrier discharge (*37*) (DBD) device installed in the

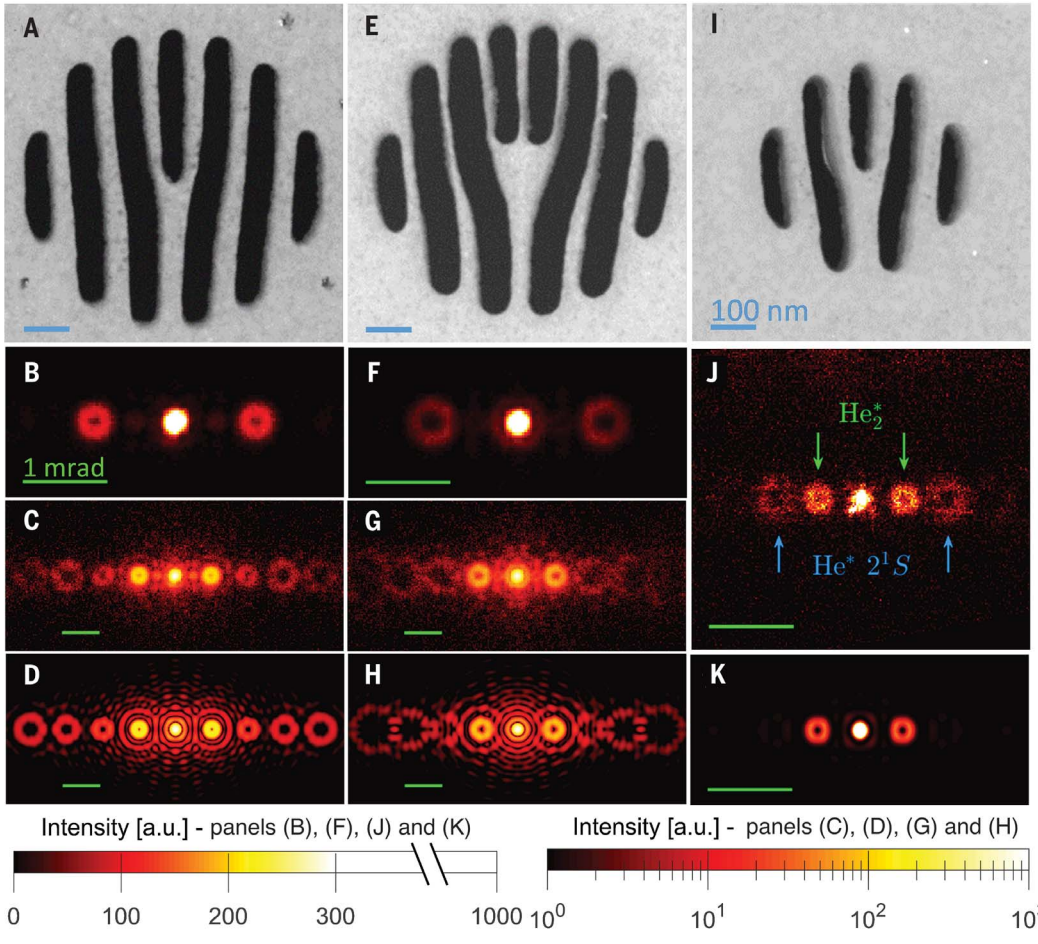

Fig. 3. Gratings and diffraction images of helium vortex beams. Experimental images were each assembled from 200,000 detected events. Theoretical images were calculated for a single grating. (**A** to **D**) A single-edge dislocation grating with a 600-nm diameter (A) produces clear rings (B) corresponding to atomic vortices with OAM of $\pm 1\hbar$ on either side of the central $l = 0$ spot. A logarithmic scale (C) reveals orders up to $l = \pm 4$ and gives a good quantitative fit to the calculated image (D). (**E** to **H**) A double-edge dislocation grating of the same size (E) produces larger diameter rings (F) with OAM of $\pm 2\hbar$, and the logarithmic scale (G) reveals the $l = \pm 4$ and ± 6 orders, as expected in the simulation (H). The logarithmic scale images [(C) and (G)] also reveal "half-order" spots resulting from metastable helium dimers, absent in the calculations [(D) and (H)]. (**I** to **K**) A smaller-diameter grating, 400 nm (I), reveals rings (J) associated with OAM-carrying dimer beams. To image the dimer vortices, the detector was distanced further from the gratings, and a resonant laser was used to deflect metastable atoms in the 2^3S state. The remaining metastable atoms in the 2^1S state appear as weak rings at twice the dimer $l = \pm 1$ diffraction angles, whereas the dimer rings give a good fit to the simulation (K). (A), (E), and (I) are scanning transmission electron microscope images. The color scale in all images is in arbitrary units. The color scale in (B), (F), (J), and (K) is saturated above 30% of the maximum intensity to emphasize the structure of the rings. The intensity in each pixel is evaluated by counting particle impacts over an area of about 900 μrad^2 in (B), (C), (F), and (G) and 400 μrad^2 in (J). Scale bars in (A), (E), and (I) are 100 nm; scale bars in (B) to (D), (F) to (H), and (J) and (K) are 1 mrad.

throat of the valve's nozzle, which applied high-voltage pulses to produce two different long-lived (metastable) excited states of atoms (*38*): 2^1S and 2^3S. These states have excess energy of about 20 eV, enabling efficient time and position-sensitive measurements using a microchannel plate (MCP) detector installed a distance $r_{GD} = 125$ cm downstream of the grating. Note that the DBD excites only a small fraction of the atoms, and therefore this method left most of the particles in the vortex beams undetected. The narrow collimation apertures and the low probability of excitation led to a recorded event rate on the order of 1 in every 50 valve pulses. The repetition rate of the experiment was set at 30 to 50 Hz, limited by the pumping speed in the source chamber and image processing.

Results

F3 Figure 3 presents accumulated images of metastable particles impacting the detector, with comparison to simulated images for single gratings. In each measured image, about 200,000 events were recorded to reveal the far-field pattern corresponding to the probability density of the diffracted matter wave. Figure 3B presents the measured diffraction image from a forked grating with a single-edge dislocation (Fig. 3A). The image contains two clear rings on either side of a central spot. Additional rings can be seen in the logarithmic scale image (Fig. 3C). The image fits well with the simulated results for this grating (Fig. 3D), with the observed rings corresponding to vortex beams with topological charges of $l = -4$ to 4. Figure 3, E to H, presents a similar measurement and calculation for a grating with a double-edge dislocation. Here, the first two rings correspond to vortex beams with topological charges $l = \pm 2$ and are therefore larger than the first-order rings of the single-edge grating. Higher even-order OAM states, up to $l = \pm 6$, are observable in the logarithmic scale images (Fig. 3, G and H).

The diffraction patterns with helium beams revealed additional diffraction spots, located between the integer diffraction orders expected for atoms. We attributed these spots to metastable helium dimers (He_2^*) produced in the valve by the DBD, which had a corresponding de Broglie wavelength half that of the atoms. Such dimers are routinely created by discharges in supersonic valves at similar source conditions (*39*), especially at low temperatures and high pressures. We verified that these additional diffraction peaks were dimers through the strong dependence of their relative intensity on these source parameters and by observing that a laser locked to a transition of the metastable atoms only transferred momentum to particles in the integer-order beams. The verification methods, which were also tested on a regular slit diffraction grating, are detailed in the supplementary materials.

Figure 3J presents the diffraction image from smaller single-edge dislocation gratings (Fig. 3I) designed for imaging the dimers. The de Broglie wavelength of these particles was half that of the atoms owing to their mass, which would lead to a correspondingly smaller diffraction image. The angular expansion of each vortex is related to the Airy disk formula

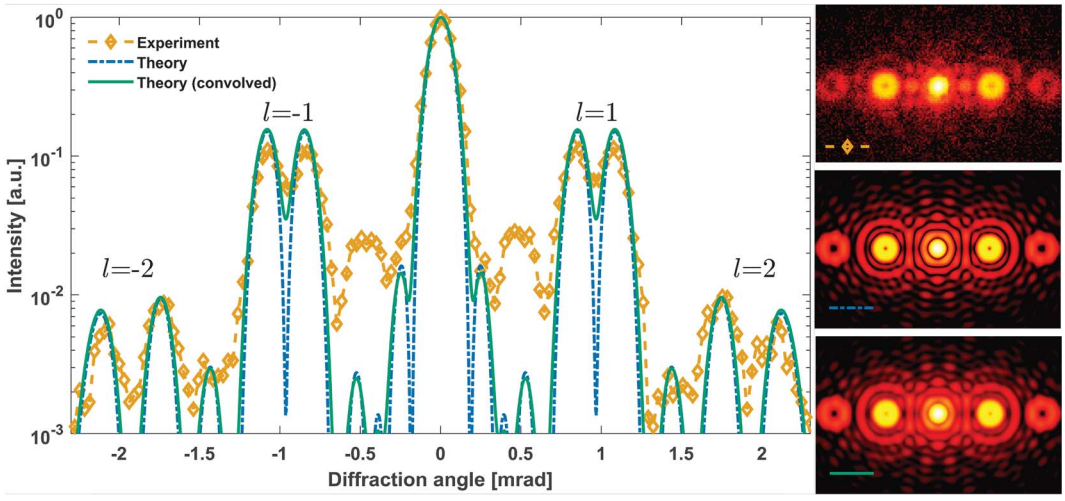

Fig. 4. Comparison of intensity measured in the experiment to theory, with simulated contribution of only the atoms. (**Left**) The intensity curves are plotted along a line crossing the helium vortex centers, shown in the range covering the l = −2 to 2 orders. Each point in the experimentally measured curve (orange) represents integration over an area 30 μrad wide (along the center line) by 90 μrad vertically. The ideal theoretical curve (blue), calculated for a monochromatic incoming wave of atoms diffracted from a single grating with an open-to-blocked slit periodicity ratio of 40/60, presents zero intensity at the center of nonzero OAM vortices. The green curve represents the ideal case with the convolution effects due to the velocity spread and the repeating grating pattern in the experiment. The latter curve shows a good fit to the experimentally measured data except for the lack of "half-order" peaks related to helium dimers. All values are given in arbitrary units normalized to the maximum intensity. (**Right**) Corresponding two-dimensional plots of the intensity for each of the three one-dimensional curves.

for the first minimum angle, $\theta \approx 1.22\lambda/a$. Therefore, we decreased the diameter of the gratings to a = 400 nm to partially compensate for the shorter wavelength. To compensate for the reduction in open area due to the smaller diameter, the gratings in this array repeated every 0.8 μm. We also installed narrower slit skimmers, with 75-μm apertures—half the value used for atoms. This was necessary to minimize incoherent blurring due to non–point source effects, also related to the divergence angle α, which become more pronounced for smaller diffraction angles. The reduction of α by half led to the same coherence length as with atoms, compensating for the doubled mass. In addition, we increased the free-flight distance from the grating to the detector to r_{GD} = 215 cm to allow for more expansion of the dimer vortex beams. Finally, the diffracted beam contains a substantial number of atoms, which would have obscured the dimer signal. One demonstrated technique for enhancing the relative contribution of dimers in a mixed beam uses another grating for mass selection (*40*). We followed an alternative method, demonstrated with sodium atoms and dimers (*41*), where a laser perpendicular to the gas beam was used to deflect the atoms out of the image. We applied a 1083-nm laser beam, resonant with the 2^3S-2^3P transition of the triplet-state metastable atoms (*42*), at 40 mW over a ~1-cm^2 spot size immediately after the grating (Fig. 2), thus scattering momentum off these atoms in the transverse direction. A small fraction of atoms, from the 2^1S state, remained in the image. Aside from this, the observed image fits well with a simulation for the dimers (Fig. 3K).

F4 Figure 4 presents a quantitative comparison of the measurements with a single-edge dislocation grating to a calculation for helium atoms. The intensity distribution is shown along a line crossing in the transverse image plane through the centers of the rings of different orders. The most appreciable discrepancy arose from the odd-order peaks of diffracted dimers, absent in the theoretical curve. For the other peaks, we improved the fit by considering that the van der Waals interaction between the grating surface and the atoms narrowed the effective width of the slits. Indeed, studies of the interactions between atoms and surfaces made from similar materials showed that van der Waals forces extend to several nanometers away from the surfaces and reduce the effective width of slits (*43*). The effect is enhanced for species with higher polarizability and is especially strong in beams of metastable helium and neon (*44*). In our results, we found an optimal fit for an effective open (transmitting) slit width of 40 nm in place of the 55 nm estimated from the scanning transmission electron microscope image. The fit was further improved by adding the contributions of blurring due to pattern repetition of the holograms and of chromatic aberration from the measured beam velocity spread.

Outlook

We have demonstrated the generation of vortex beams of atoms and molecules with intrinsic OAM. To our knowledge, this is the first successful demonstration of vortices of nonelementary particles. The experiment was enabled by the production of beams with a relatively large coherence length, comparable to the dimensions of the nanometric grating. The method could be applied to most gaseous species owing to the generality of the supersonic valve apparatus (for example, see our measurement of neon vortices in the supplementary materials). Although heavy species require collimation with narrower skimmers to achieve sufficient transverse coherence length, and possibly the use of a carrier gas for efficient expansion cooling, there is no fundamental limit on the mass that can be used (*45*). Supersonic beams are also a convenient source for creating charged beams, through ionization of the atoms. In this manner, it would be possible to form a charged vortex beam of various particles, which could provide an extension to applications of electron vortex beams (*46*). A particularly interesting case would be to create OAM beams of protons by ionizing atomic hydrogen, a prospective path to studying the proton's internal structure through the coupling of the internal charge distribution with the twisting wavefunction of the center of mass (*22*).

The fabrication method we established can be used to design other holograms for wavefront shaping of matter waves, which could yield a broad range of potential applications; for example, matter waves may be shaped in such a manner that they will pull a collision target instead of pushing it (*47*). In low-energy scattering experiments between atoms and/or molecules, wavefront shaping would open an entirely new frontier. To date, in all such realizations with well-defined low collision energy (*38*, *48*, *49*), the scattering partners are well described by single momentum values, i.e., plane waves. There is often a certain variance of momenta value (transversely and longitudinally), but it is considered as an incoherent distribution rather than a coherent superposition as in our case. OAM beams would introduce helicity to these otherwise axisymmetric probes and may allow one to explore chiral interactions with various molecular partners.

Conversely, the vortex-generating mask itself may be used as a probe for OAM in scattering experiments. Here, particles exiting a collision are diffracted from a grating, and any preexisting OAM will lead to an asymmetric intensity

image, as demonstrated in OAM sorters of electron beams (*50*). In this manner, it would be possible to observe hitherto unexplored properties of reactions or other collisions between atoms or molecules. This concept of identifying OAM resulting from scattering experiments can be generalized beyond atomic physics: OAM sorters can be used in high-energy physics to extract new types of information from scattering processes, about chirality and generally regarding the role of transverse wave functions in altering fundamental interactions (*51*).

Finally, the OAM of matter waves may be used to try to modify selection rules in light-matter interactions. The probability of absorbing light through an atomic transition is dependent on the angular momentum of the photon and on the total angular momentum of the atomic state before and after the transition. Previous works have shown how creating vortex beams of photons can alter selection rules in transitions of trapped ions, with the intrinsic OAM of the photons contributing to the total angular momentum balance (*52*). Instead of the photons, we propose shaping the massive particles as vortices to examine the coupling strength of the matter wave OAM with other degrees of freedom. Experimental signatures of such an experiment would be, for example, the observation of an electronic transition that would otherwise be forbidden. This approach could be expanded by exciting the atoms to Rydberg states, where the vortex extent and the internal dimensions of the electron wave functions in the atoms are comparable. Taking these ideas to light-matter interactions of molecules could couple the OAM degree of freedom to the complexity of molecular rotations, creating hybrid rotational states that combine the quantum states of the nuclei and the center of mass.

REFERENCES AND NOTES

1. L. M. Milne-Thomson, *Theoretical Hydrodynamics* (Macmillan, 1968).
2. D. R. Tilley, J. Tilley, *Superfluidity and Superconductivity* (Adam Hilger, 1990).
3. R. N. Zare, *Angular Momentum: Understanding Spatial Aspects in Chemistry and Physics* (Wiley, 1988).
4. M. R. Matthews *et al*., *Phys. Rev. Lett.* **83**, 2498–2501 (1999).
5. K. W. Madison, F. Chevy, W. Wohlleben, J. Dalibard, *Phys. Rev. Lett.* **84**, 806–809 (2000).
6. J. R. Abo-Shaeer, C. Raman, J. M. Vogels, W. Ketterle, *Science* **292**, 476–479 (2001).
7. L. Allen, M. W. Beijersbergen, R. J. C. Spreeuw, J. P. Woerdman, *Phys. Rev. A* **45**, 8185–8189 (1992).
8. H. He, M. E. J. Friese, N. R. Heckenberg, H. Rubinsztein-Dunlop, *Phys. Rev. Lett.* **75**, 826–829 (1995).
9. G. C. G. Berkhout, M. W. Beijersbergen, *J. Opt. A Pure Appl. Opt.* **11**, 094021 (2009).
10. J. T. Barreiro, T. C. Wei, P. G. Kwiat, *Nat. Phys.* **4**, 282–286 (2008).
11. M. J. Padgett, *Opt. Express* **25**, 11265–11274 (2017).
12. Y. Shen *et al*., *Light Sci. Appl.* **8**, 90 (2019).
13. K. Y. Bliokh *et al*., *Phys. Rep.* **690**, 1–70 (2017).
14. M. Uchida, A. Tonomura, *Nature* **464**, 737–739 (2010).
15. J. Verbeeck, H. Tian, P. Schattschneider, *Nature* **467**, 301–304 (2010).
16. S. Lloyd, M. Babiker, J. Yuan, *Phys. Rev. Lett.* **108**, 074802 (2012).
17. J. Verbeeck, H. Tian, G. Van Tendeloo, *Adv. Mater.* **25**, 1114–1117 (2013).
18. J. Harris *et al*., *Nat. Phys.* **11**, 629–634 (2015).
19. S. M. Lloyd, M. Babiker, G. Thirunavukkarasu, J. Yuan, *Rev. Mod. Phys.* **89**, 035004 (2017).
20. S. Gargiulo, I. Madan, F. Carbone, Nuclear excitation by electron capture in excited ions. arXiv:2102.05718v1 [nucl-th] (2021).
21. H. Larocque, I. Kaminer, V. Grillo, R. W. Boyd, E. Karimi, *Nat. Phys.* **14**, 1–2 (2018).
22. G. M. Vanacore *et al*., *Nat. Mater.* **18**, 573–579 (2019).
23. V. E. Lembessis, D. Ellinas, M. Babiker, O. Al-Dossary, *Phys. Rev. A* **89**, 053616 (2014).
24. I. Madan, G. M. Vanacore, S. Gargiulo, T. LaGrange, F. Carbone, *Appl. Phys. Lett.* **116**, 230502 (2020).
25. C. W. Clark *et al*., *Nature* **525**, 504–506 (2015).
26. R. L. Cappelletti, T. Jach, J. Vinson, *Phys. Rev. Lett.* **120**, 090402 (2018).
27. S. S. R. Oemrawsingh *et al*., *Appl. Opt.* **43**, 688–694 (2004).
28. A. Béché, R. Winkler, H. Plank, F. Hofer, J. Verbeeck, *Micron* **80**, 34–38 (2016).
29. N. R. Heckenberg, R. McDuff, C. P. Smith, H. Rubinsztein-Dunlop, M. J. Wegener, *Opt. Quantum Electron.* **24**, S951–S962 (1992).
30. U. Even, J. Jortner, D. Noy, N. Lavie, C. Cossart-Magos, *J. Chem. Phys.* **112**, 8068–8071 (2000).
31. D. W. Keith, M. L. Schattenburg, H. I. Smith, D. E. Pritchard, *Phys. Rev. Lett.* **61**, 1580–1583 (1988).
32. J. Fujita *et al*., *Nature* **380**, 691–694 (1996).
33. M. Arndt *et al*., *Nature* **401**, 680–682 (1999).
34. C. Brand *et al*., *Nat. Nanotechnol.* **10**, 845–848 (2015).
35. A. R. Barnea, O. Cheshnovsky, U. Even, *Phys. Rev. A* **97**, 023601 (2018).
36. C. Keller, J. Schmiedmayer, A. Zeilinger, *Opt. Commun.* **179**, 129–135 (2000).
37. K. Luria, N. Lavie, U. Even, *Rev. Sci. Instrum.* **80**, 104102 (2009).
38. A. B. Henson, S. Gersten, Y. Shagam, J. Narevicius, E. Narevicius, *Science* **338**, 234–238 (2012).
39. M. Raunhardt, M. Schäfer, N. Vanhaecke, F. Merkt, *J. Chem. Phys.* **128**, 164310 (2008).
40. W. Schöllkopf, J. P. Toennies, *Science* **266**, 1345–1348 (1994).
41. M. S. Chapman *et al*., *Phys. Rev. Lett.* **74**, 4783–4786 (1995).
42. M. R. Wehr, *Phys. Rev.* **39**, 796–801 (1932).
43. R. E. Grisenti, W. Schöllkopf, J. P. Toennies, G. C. Hegerfeldt, T. Köhler, *Phys. Rev. Lett.* **83**, 1755–1758 (1999).
44. R. Brühl *et al*., *Europhys. Lett.* **59**, 357–363 (2002).
45. Y. Y. Fein *et al*., *Nat. Phys.* **15**, 1242–1245 (2019).
46. D. Karlovets, *New J. Phys.* **23**, 033048 (2021).
47. A. A. Gorlach, M. A. Gorlach, A. V. Lavrinenko, A. Novitsky, *Phys. Rev. Lett.* **118**, 180401 (2017).
48. S. N. Vogels *et al*., *Science* **350**, 787–790 (2015).
49. J. Jankunas, K. Jachymski, M. Hapka, A. Osterwalder, *J. Chem. Phys.* **142**, 164305 (2015).
50. A. H. Tavabi *et al*., *Phys. Rev. Lett.* **126**, 094802 (2021).
51. I. Kaminer *et al*., *Phys. Rev. X* **6**, 011006 (2016).
52. C. T. Schmiegelow *et al*., *Nat. Commun.* **7**, 12998 (2016).
53. A. Luski *et al*., Vortex beams of atoms and molecules. Zenodo (2021); https://doi.org/10.5281/zenodo.4917316.

ACKNOWLEDGMENTS

We acknowledge I. Kaplan-Ashiri for professional support in providing the STEM images. **Funding:** European Research Council H2020 Program and the Minerva Foundation. **Author contributions:** A.L., Y.S., R.D., and E.N. designed, constructed, and conducted the experiment and analyzed the results. A.R.B. provided designs for essential parts. O.B., H.N., A.R.B., and O.C. developed the fabrication process and prepared the gratings. O.C. contributed to the development of experimental methodology. A.L., Y.S., E.N., I.K., and A.G. contributed to the conception of the project. **Competing interests:** The authors declare that they have no competing interests. **Data and materials availability:** All data underlying the figures are deposited at Zenodo (*53*).

SUPPLEMENTARY MATERIALS

science.sciencemag.org/content/373/6559/1105/suppl/DC1
Materials and Methods
Supplementary Text
Figs. S1 to S6
Table S1

29 April 2021; accepted 24 June 2021
10.1126/science.abj2451

Science

Vortex beams of atoms and molecules

Alon LuskiYair SegevRea DavidOra BittonHila NadlerA. Ronny BarneaAlexey GorlachOri CheshnovskyIdo KaminerEdvardas Narevicius

Science, 373 (6559), • DOI: 10.1126/science.abj2451

Vortex beams of nonelementary particles

The discovery of photon and electron vortex beams carrying orbital angular momentum (as a result of a twisting wave front) has led to appreciable advances in optical imaging, optical and electron microscopy, communications, quantum optics and micromanipulation, and more advances are expected. In an effort to extend this progress to other types of beams, Luski *et al*. demonstrate the production of vortex beams of helium atoms and dimers formed from supersonic beams with large coherence lengths diffracted off of specifically nanofabricated gratings with fork dislocations (see the Perspective by Kornilov). Vortex beams made of nonelementary particles with internal degrees of freedom represent a direct manifestation of quantum mechanics on macroscopic scale, and their production paves the way for many long-awaited applications. —YS

Science (ISSN) is published by the American Association for the Advancement of Science. 1200 New York Avenue NW, Washington, DC 20005. The title *Science* is a registered trademark of AAAS.